Lidar Observation of a Mixed-Phase Altostratus Cloud

C. M. R. PLATT[1]

Division of Atmospheric Physics, CSIRO, Aspendale, Victoria, Australia, 3195

(Manuscript received 8 September 1976, in revised form 15 March 1977)

ABSTRACT

Measurements by monostatic lidar of linear depolarization ratios and backscatter coefficients in an altostratus cloud revealed a horizontally layered structure. Three different types of layers were observed. The bottom and central layers had depolarization ratios varying from 0.3 to 0.4, which identified them as layers containing mainly ice. The backscatter coefficients were similar to those found in cirrus ice clouds. A central, transient layer had depolarization ratios characteristic of a high-density water cloud, although the total integrated backscatter of 2.3 ± 1.2 was high for this type of cloud. The top layer had a depolarization ratio of 0.2 at the cloud base, decreasing to 0.04 at the cloud center. Backscatter coefficients ranged up to 30 km^{-1} and the total integrated backscatter was about 7.6 ± 3.8. This value is considerably higher than the range of values predicted for water or cirrus ice clouds and one possible explanation is that specular reflection was occurring from horizontally aligned ice crystal plates.

The variation of backscatter coefficient within each layer was rather regular, with a maximum at the center of the layers. The cloud was situated in a stable air stream and its evolution appeared to be slow.

1. Introduction

The potential of lidar depolarization for discrimination between water, ice and mixed phases in clouds was recognized by Schotland *et al.* (1971) who observed appreciable depolarization of a linearly polarized lidar beam by ice crystals. Although depolarization ratios approaching unity have been observed in some ice clouds, they are typically about 0.4. Sassen (1974) has since shown that the depolarization ratio is dependent on the ratio of ice crystal to water droplet concentration. The theoretical value of the depolarization ratio for water spheres in the back direction is zero (Liou and Schotland, 1971), while the measured value near the bases of water cloud is about 0.03 (Sassen, 1974). However, for any appreciable cloud thickness, the depolarization ratio is found to increase almost linearly with increasing cloud penetration, reaching values of 0.4–0.5 within a depth of about 150 m (Pal and Carswell, 1973). This effect is due to multiple scattering of radiation in the lidar beam, although theoretical studies have as yet been unable to simulate the measured figures (e.g., Eloranta 1972; Liou and Schotland, 1971).

Depolarization measurements can be usefully supplemented by measurements of the backscatter coefficients of the clouds. Platt (1973) has shown that the integrated backscatter from a cloud tends, as the cloud becomes denser, to a value which is related by a constant factor to the backscatter to extinction ratio of the cloud particles. This quantity varies with cloud phase and type (Platt and Bartusek, 1974).

Recently a high-power ruby lidar system was installed at Aspendale with facilities for depolarization studies and fast digitization of data. Preliminary measurements of depolarization ratios in cirrus and water clouds have broadly verified the work of other authors. These results will be published elsewhere. Here we report some interesting observations of depolarization ratios and backscatter coefficients from one altostratus cloud system which showed a vertical structure of distinct layers with differing optical properties.

2. Instrumental and experimental technique

The Aspendale system is a monostatic lidar with facilities for rapid comparison between normal and depolarized returns. The ruby laser has an output energy of 1.5 J and a pulse width of 20 ns. The maximum pulse rate is 1 s^{-1}. The reflected light is imaged by a 14-inch Celestron telescope. The polarizer is placed near the telescope focus and can be rotated rapidly between pulses. The photomultiplier output voltage is digitized by a BIOMATION 8100 Recorder with a minimum sampling time of 10 ns. A 2100 Hewlett–Packard computer controls the laser firing time and the transfer of data to tape. The pulse energy is also measured and recorded and received amplitudes are normalized to unity pulse energy. Returns from cloud were calibrated by comparison with returns from

[1] Present affiliation: Cooperative Institute for Research in Environmental Sciences, University of Colorado/NOAA, Boulder, Colo. 80309 (until September 1977).

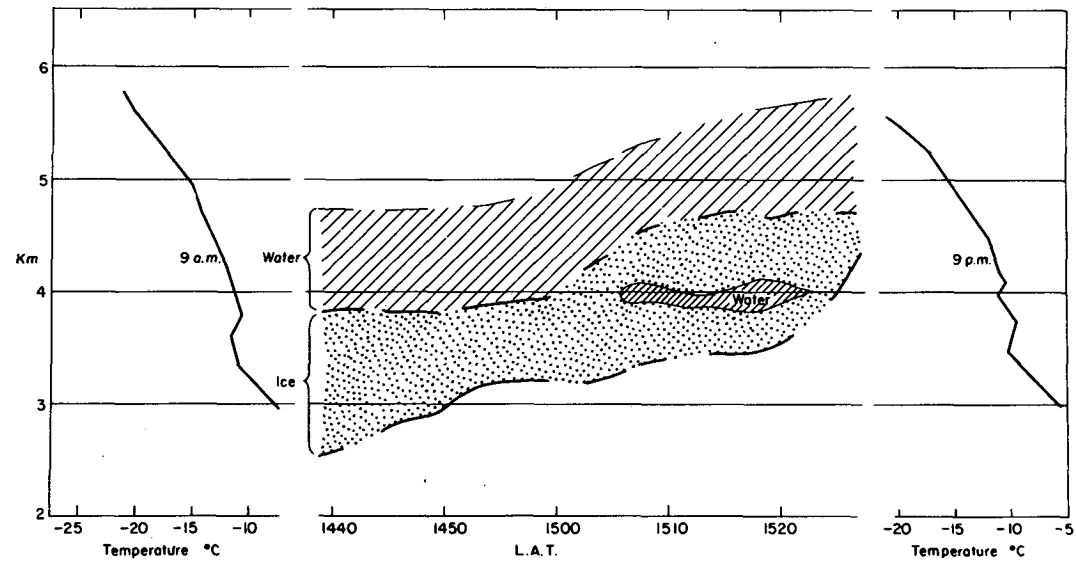

FIG. 1. Time-height representation of the altostratus cloud over the total time of observation. The dashed contours indicate the main separation of the different phases when data were available. The designation of phase is only tentative. Radiosonde temperature profiles are shown at 0900 and 2100 local apparent time.

dust-free air of known backscatter coefficient and corrected for attenuation between the cloud and ground (Platt, 1973). The estimated error in calibration was $\pm 25\%$.

For the present experiment the lidar was fired in the vertical every 5s and between each pulse the polarizer was rotated through 90°. This was the minimum rate achievable at the time of the experiment. The optimum rate of rotation of the polarizer of 1 s^{-1} has since been achieved. The output voltage from the photomultiplier was sampled by the BIOMATION recorder at 20 ns intervals. The transmitted lidar pulse had a beamwidth of 1 mrad and the receiver system beamwidth was adjusted to 10 mrad. The wide receiver aperture enabled better penetration of the cloud via multiple scattering processes (Platt, 1973).

3. Analysis of data

The depolarization ratio $\delta(z)$ at altitude z is given by Schotland *et al.* (1971) as

$$\delta(z)=\frac{B(\pi,z)_{\perp}}{B(\pi,z)_{\parallel}}[\exp(\tau_{\parallel}-\tau_{\perp})], \qquad (1)$$

where $B(\pi,z)_{\perp}$ and $B(\pi,z)_{\parallel}$ are the backscatter coefficients at altitude z for the perpendicular and parallel polarized returns, respectively. The exponential term allows for a difference in cloud transmittance for the two components due to, say, preferentially aligned ice crystals, but here as in Schotland *et al.* (1971) it will be taken as unity. If the crystals are not oriented, then they would present the same mean extinction cross section to either polarization. The transmittance could possibly be affected by differences in the angular scattering functions in the back hemisphere affecting the two multiple scattered returns, but again the random orientation of the crystals would be expected to partially smooth out such differences.

In this case, $\delta(z)$ is given simply by the ratio of the return intensities $P_{\perp}(z)$ and $P_{\parallel}(z)$ at the lidar receiver. It is noted that other terms in the lidar equation such as range, receiver gain, etc., do not appear in the expression for $\delta(z)$.

A first viewing of the values of $P_{\perp}(z)$ and $P_{\parallel}(z)$ revealed a situation where cloud properties were varying slowly in the interval between firings. To allow for a linear change of $P_{\parallel}(z)$ within the 10 s between observations of this quantity $\delta(z)$ was defined as the ratio of $P_{\perp}(z)$ at time t seconds to the mean of $P_{\parallel}(z)$ $(t-5)$ and $P_{\parallel}(z)$ $(t+5)$. The data, which were stored on tape, were processed by computer to give values of the quantities $\delta(z)(t)$ and $\frac{1}{2}[P_{\parallel}(z)(t-5)+P_{\parallel}(z)(t+5)]$ at time intervals of 10 s minimum.

4. Observations

Lidar returns were obtained from an altostratus cloud during the period from 1438 to 1525 hours[2] on 9 August 1975. The returns were obtained sufficiently often to build up time-height cross sections of the cloud as shown in Figs. 1 and 2. Periods when observations were not made are shown as breaks in the line defining the cloud base. The designations of the cloud phases in Figs. 1 and 2 are only very tentative, being based on previous depolarization results reported by other workers, as discussed in Section 1. The analysis of the integrated backscatter, which is discussed in

[2] Local apparent time.

Section 5b, casts doubt on the reality of some of the above designations.

The current synoptic map showed a large, complex, low-pressure system centered about 600 km east of Aspendale. A front had passed through Aspendale during the previous 24 h and the cloud was situated in a rather stable air mass behind the front. This stability is evident in the temperature profiles illustrated in Fig. 1 which were measured by radiosonde at Laverton, some 40 km west of Aspendale.

5. Discussion of results

The discussion of the cloud observations is divided for convenience into three sections. In Section 5a the depolarization patterns from some single lidar returns during the period 1518 to 1524 are discussed in detail, and the phases of the particles in the layers are interpreted in terms of these patterns. In Section 5b, the backscatter coefficients and the integrated backscatter are evaluated and discussed for different layers and for the same period as Section 5a. Section 5c is devoted to a discussion of the cloud structure and its evolution as it passed through the lidar's field of view.

a. Interpretation of depolarization patterns

Four displays are shown in Figs. 3a–3d which indicate the patterns in the backscatter and depolarization observed between 1518 and 1524.

The "noise" evident in the depolarization ratio is due not only to photon noise in the original returns but also to the limited resolution of the BIOMATION recorder. The output of this instrument was restricted to 0–128 counts. When the backscatter returns from the most intense layers were matched to the upper end of this range, the returns from the weaker ice layers measured about 10 counts in the case of $B_{\parallel}$ and only about 4 in $B_{\perp}$. The "noise" in $\delta(z)$ caused by this effect was thus about 25%.

Fig. 3a shows the return from a layer of cloud with its base at an altitude of 3.35 km and with a depolarization ratio of about 0.4, which is typical for an ice cloud containing very little, or no, water (Sassen, 1974). Overlying this layer, at an altitude of 3.70 km, is a highly reflecting layer with a very low value of $\delta(z)$ of about 0.03. The layer is thus identified as a water cloud. A second layer immediately above it is also highly reflecting but has an increasing depolarization ratio with increasing altitude. These characteristics identify the layer from past work as a dense water cloud with a high extinction coefficient (Pal and Carswell, 1973). The depolarization behavior, coupled with an absence of returns from above this layer, points to complete extinction of the lidar pulse.

Fig. 3b shows the situation 1 min after that depicted in Fig. 3a. The lower water layer has disappeared and the layer at 3.90 km has both a smaller depth and backscatter coefficient. As a result, the laser pulse can now penetrate the water layers to reveal two further layers above. The first extends from about 3.9 to 4.5 km and appears to be an ice layer. The second extends from about 4.5 to 5.4 km and within this range, the depolarization ratio decreases to a low value.

After a further minute and three-quarters (Fig. 3) the lower water layer at 3.8 km has nearly disappeared and the topmost layer is seen to be nearly 1 km deep. The backscatter from the layers above 3.8 km has increased in intensity which can be attributed to the

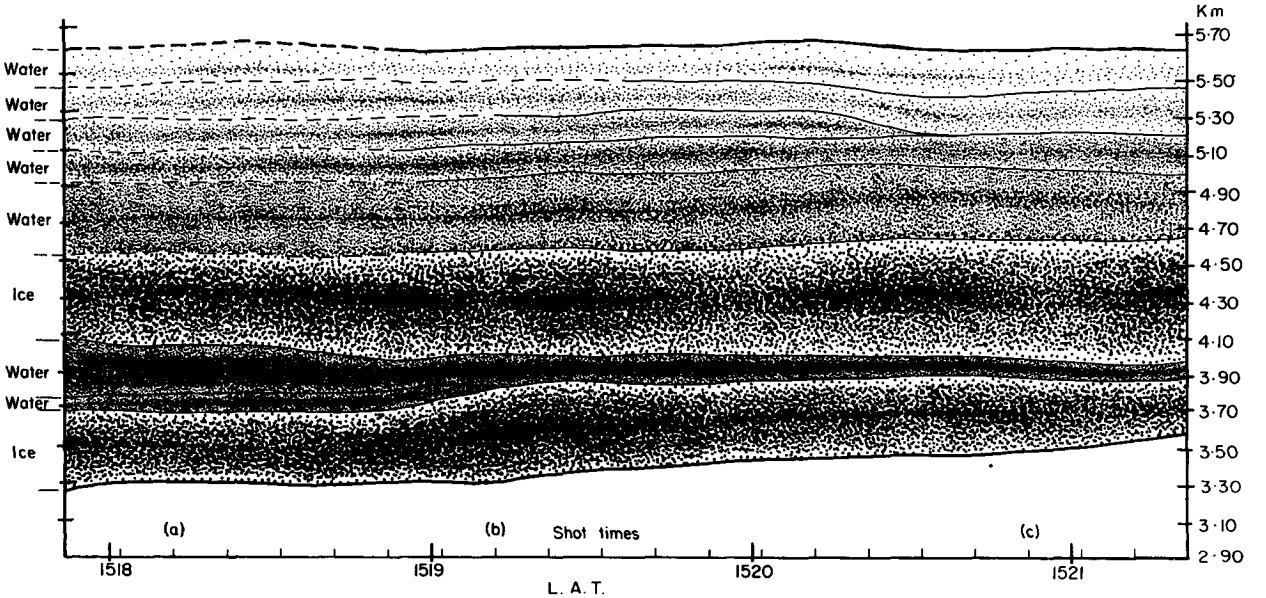

FIG. 2. Time-height representation of the cloud evolution from 1518 to 1522 hours 9 August 1975. Times of depolarized returns are shown on the horizontal axis. Parallel returns were received at intermediate times. The letters in brackets refer to depolarized returns used in Figs. 3a–3c. The representation of the layer intensities is only qualitative, and the phase designation is tentative.

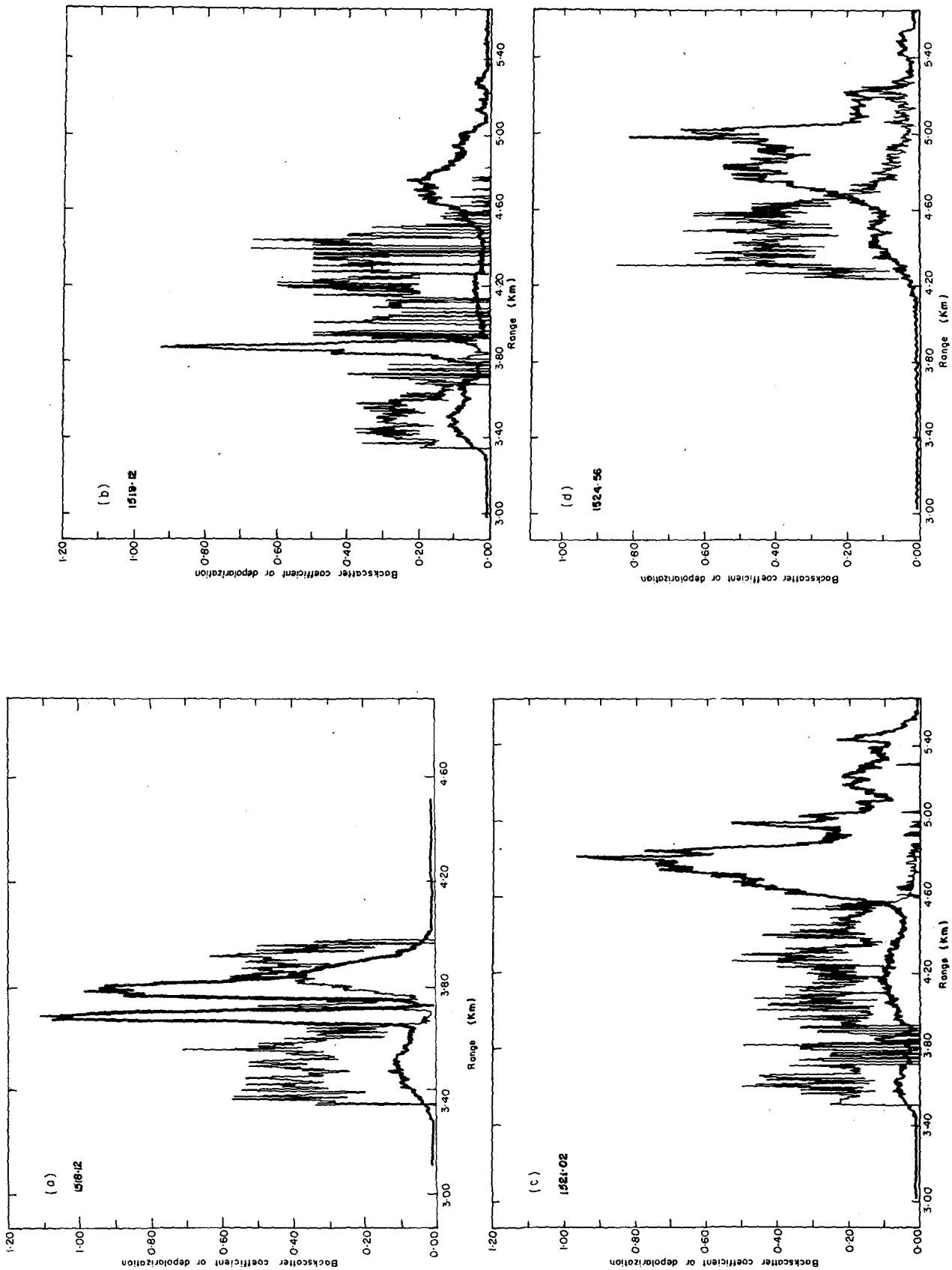

FIG. 3. Altitude dependence of backscatter coefficient and depolarization ratio at four local apparent times on 9 August 1975. Backscatter coefficient is shown as the fuller line and the units are km^{-1} when the vertical scale is multiplied by 10.

decreased extinction below these layers. Above 4.6 km the depolarization is apparently very small, which would indicate that this layer was also composed of small water drops. However, the zero value of $\delta(z)$ above 5 km is a result of the small depolarized returns from this region being unresolvable by the BIOMATION recorder. These returns can be better resolved if a logarithmic amplifier is used at the output of the lidar receiver photomultiplier and such a return is shown in Fig. 3d. Here $\delta(z)$ is seen to fall to a value of about 0.04 at 5 km. It is interesting that between 4.8 and 5 km, $\delta(z)$ gradually decreases, signifying a slow change in the cloud composition from a predominantly ice layer to what is apparently a water layer (Sassen, 1974).

b. Interpretation of backscatter characteristics of layers

The above identification of cloud layers purely in terms of their depolarization ratios is based on previous work. Additional information on the nature of the cloud layers is available from measured backscatter coefficients and calculations of the integrated backscatter. The following analysis indicates that this information contradicts, in some aspects, designation of the "water" layers in Figs. 1 and 2.

The total backscatter coefficient $B(\pi)$ is equal to the sum of $B(\pi)_{11}$ and $B(\pi)_{\perp}$. The *measured* backscatter $B'(\pi,z)$, at range (altitude) z is less, due to attenuation of the lidar pulse during its passage through the cloud. Thus

$$B'(\pi,z)=B(\pi,z)\exp\left[-\int_{z_0}^{z}2\eta(z'')\sigma(z'')dz''\right], \quad (2)$$

where z_0 is cloud-base altitude, $\eta(z'')$ a multiple scattering factor and $\sigma(z'')$ the cloud extinction coefficient. It is assumed that $\sigma(z'')$ and $\eta(z'')$ are both equal for the two polarization directions.

A quantity $\gamma'(\pi)$ is defined in Platt (1973) as

$$\gamma'(\pi)=\int_{z_0}^{h}B'(\pi,z)dz, \quad (3)$$

where h is cloud top altitude. If it is assumed that $\eta(z'')$ $[=\eta]$ is constant, then substitution of (2) into (3) and integrating gives

$$\gamma'(\pi)=(k/2\eta)[1-\exp(-2\eta\tau_v)], \quad (4)$$

where

$$\tau_v=\int_{z_0}^{h}\sigma(z'')dz'' \quad \text{and} \quad k=B(\pi,z)/\sigma(z).$$

The assumption that η is constant is not always valid (Kunkel and Weinman, 1976). However, Eq. (4) is convenient for the analysis of cloud data. When τ_v becomes large, $\gamma'(\pi)$ tends to $k/2\eta$. Thus, a series of measurements of $\gamma'(\pi)$ for different values of τ_v can give an experimental value of $k/2\eta$ (Platt, 1973). If η is not constant then an effective value, $k/2\bar{\eta}$, is measured where

$$\bar{\eta}=\frac{1}{2}\int_{z_0}^{h}k\sigma(z)\left[\exp-\int_{z_0}^{z}2\eta(z'')\sigma(z'')dz''\right]dz. \quad (5)$$

Although relatively few determinations of $k/2\bar{\eta}$ have been made, its value was found to lie between 0.3 and 0.6 for several different cirrus and cirrostratus systems (Platt, 1973; and unpublished data), and that a similar range of values occurred in some middle-level clouds (Platt and Bartusek, 1974). Some of this variation was due to the use of different receiver beamwidths, which varied between 3 and 10 mrad. $\bar{\eta}$ would decrease with increasing beamwidth. Also, those authors calculated theoretical values of k for two water clouds as 0.64 and 0.67, respectively. The corresponding value of $\bar{\eta}$ for water clouds is estimated to lie between 0.6 and 0.9 (Kunkel and Weinmann, 1976), so that $k/2\bar{\eta}$ for water clouds is predicted to lie within the range of 0.36 to 0.54. However, with the wide receiver beamwidth of 10 mrad, the value of $\bar{\eta}$ is likely to be at the low end of the quoted range.

The relevance of the above discussion to the present article is that some of the values of $\gamma'(\pi)$ determined for different layers in the altostratus cloud were considerably higher than any of the above quoted values, even allowing for an estimated 50% error. Values of $\gamma'(\pi)$ are listed in Table 1. Some of the layers overlap because values were calculated from two separate lidar returns, as indicated. Except for layer 2, none of the layers were opaque to the lidar pulse so that values of $\gamma'(\pi)$ [Eq. (4)] for layers 1, 3 and 4 were actually *less* than the corresponding values of $k/2\bar{\eta}$. Values of $\gamma'(\pi)$ for each layer above the first were corrected for attenuation by the layers beneath, using the mean value of $k/2\bar{\eta}$ (the effective backscatter to extinction ratio) measured for cirrus.

Layers 1 and 3 had backscatter (and depolarization) values which were similar to those of cirrus clouds. However, layers 2 and 4 had backscatter values which were respectively about 2–4 times and 8–16 times the predicted theoretical values for water clouds. Despite assumptions made about the behavior of $\eta(z)$ or the transmittance of the layers, layers 2 and 4 apparently

TABLE 1. Integrated backscatter through different layers of the altostratus cloud.

Layer No.	Figure No.	Altitude (km)	$\gamma'(\pi)$	$\gamma'(\pi)$*
1	3a	3.3 –3.65	0.17	0.17±0.04
2	3a	3.75–4.0	1.42	2.3 ±1.2
3	3c	3.85–4.6	0.36	0.6 ±0.3
4	3c	4.6 –5.6	2.30	7.6 ±3.8

* Corrected for attenuation below the layer.

possess backscatter characteristics which are different from those of either cirrus or water clouds, while their depolarization characteristics are similar to those of water clouds. Thus the interpretation of the layers solely in terms of their depolarization characteristics must be called into question. It is still possible that layer 3 could have been a water cloud. It was very dense, and attenuated the lidar pulse within a few hundred meters. This interpretation could imply that $\gamma'(\pi)$ was in error by more than 100%, which is a possibility. However, the value of $\gamma'(\pi)$ for layer 4 was more than an order of magnitude greater than that predicted for a water cloud and even then the layer did not seem to attenuate the lidar pulse completely. A possible explanation for the high backscatter was that reflection was occurring from horizontally aligned hexagonal ice plates. The observed temperature range in layer 4 (-12 to -20°C) was just that range in which hexagonal ice plates form. The low depolarization ratio would also be consistent with this explanation (Liou and Lahore, 1974). Scattering by ice plates will be explored further in a subsequent paper. Suffice it to say here that a low depolarization ratio may *not necessarily* imply automatically a cloud of water droplets.

c. *Cloud structure and evolution*

In the time-height representations of Figs. 1 and 2, spatial and temporal variations in cloud structure could not be separated. However, there are reasons for thinking that most of the variations were spatial. Although the cloud was situated in a complex low-pressure system it was not in an active frontal zone, but in an area of stability to the rear of a front. Clouds in such a region are often in a mature phase of growth and layered in structure (Borovikov *et al.*, 1963; Mason, 1971). Ascending motions are rather weak ($\sim$1 cm s^{-1}) and cloud evolution is accordingly quite slow. This would be particularly true for mature ice layers, such as the bottom layer in Fig. 2, which are known to evolve more slowly than water clouds.

An interesting feature of the cloud structure is the local maximum in cloud backscatter coefficient which tends to occur at the center of each layer. This structure is shown best in Fig. 3c, particularly for the ice layers. Assuming that the cloud particle size distribution was constant with height in each layer, the variation in backscatter coefficient would imply similar variations in both the particle number density and the cloud water content. One possible explanation for this structure is that the cloud initially formed in thermally stratified air in which there was a variation in cloud condensation nuclei. Certainly, on the day of observation, the temperature profiles indicated considerable stratification (Fig. 1) at cloud height. Another factor which might be important is variations in shear-induced mechanical mixing.

In contrast to the generally stable nature of the cloud, the dense "water" layer observed between 1506 and 1521 at about 3.8 km must have represented a local active growth phase in the cloud. The top of this layer was probably defined by the temperature inversion near 4 km.

6. Summary

Layers with very different optical properties have been observed in an altostratus cloud using a calibrated lidar with depolarization facilities. The identification of the layers as given in Figs. 1 and 2 is necessarily very tentative due to a lack of any definitive set of lidar measurements coupled with simultaneous direct sampling of cloud particles. Furthermore, the measured integrated backscatter casts doubt on whether those layers which gave a small depolarization ratio were actually water drop clouds. Very high backscatter coefficients, coupled with a low depolarization ratio, were observed in the top cloud layers, which had air temperatures varying from -12 to -20°C. A possible explanation advanced to explain these properties is that reflection was occurring from horizontally aligned ice plates.

The measurement of the integrated backscatter $\gamma'(\pi)$ is obviously an important additional quantity in the interpretation of cloud lidar depolarization measurements; for instance, the above observations indicate that a low depolarization ratio may not unambiguously identify a water cloud.

One method of testing the hypothesis of specular reflection from ice crystals would be to take lidar measurements at various angles to the vertical. If specular reflection was occurring, then the measured lidar backscatter would decrease dramatically as the lidar was scanned away from the vertical.

Other interesting features observed in the cloud were the highly opaque, transient "water" layers in the center of the cloud and the regular variations of backscatter within each layer. In fact, each layer was bounded and defined by regions of low backscatter.

In order to make the integrated backscatter measurements more definitive, the dependence of $\bar{\eta}$ and depolarization ratio on receiver beamwidth and cloud type is at present under study, both theoretically and experimentally.

Acknowledgment. Thanks are due to Mr. A. C. Dilley for his substantial contributions to the programming of the lidar data acquisition system and the reduction of the data.

REFERENCES

Borovikov, A. M., A. Kh. Khrgian, and others, 1963: *Cloud Physics.* [Israel Program for Scientific Translations, 329 pp.]

Eloranta, E., 1972, Calculation of doubly scattered lidar returns. Ph.D. thesis, University of Wisconsin, 115 pp.

Kunkel, K. E., and J. A. Weinmann, 1976, Monte Carlo analysis of multiply scattered lidar returns. *J. Atmos. Sci.*, **33**, 1772–1781.

Liou, Kuo-Nan, and R. M. Schotland, 1971: Multiple backscattering and depolarization from water clouds for a pulsed laser system. *J. Atmos. Sci.*, **28**, 772–784.

——, and H. Lahore, 1974: Laser sensing of cloud composition: A backscattered depolarization technique. *J. Appl. Meteor.*, **13**, 257–263.

Mason, B. J., 1971, *The Physics of Clouds*, 2nd ed. Oxford University Press, 671 pp.

Pal, S. R., and A. I. Carswell, 1973, Polarization properties of lidar backscattering from clouds. *Appl. Opt.*, **12**, 1530–1535.

Platt, C. M. R., 1973, Lidar and radiometric observations of cirrus clouds. *J. Atmos. Sci.*, **30**, 1191–1204.

——, and K. Bartusek, 1974: Structure and optical properties of some middle-level clouds. *J. Atmos. Sci.*, **31**, 1079–1088.

Sassen, K., 1974, Depolarization of laser light backscattered by artificial ice clouds. *J. Appl. Meteor.*, **13**, 923–933.

Schotland, R. M., K. Sassen and R. Stone, 1971: Observations by lidar of linear depolarization ratios for hydrometeors. *J. Appl. Meteor.*, **10**, 1011–1017.